Quantum-walk approach to searching on fractal structures

E. Agliari*

Dipartimento di Fisica, Università degli Studi di Parma, viale Usberti 7/A, I-43100 Parma, Italy and
Theoretische Polymerphysik, Universität Freiburg, Hermann-Herder Strasse 3, D-79104 Freiburg, Germany

A. Blumen and O. Mülken

Theoretische Polymerphysik, Universität Freiburg, Hermann-Herder Strasse 3, D-79104 Freiburg, Germany

(Received 23 April 2009; revised manuscript received 8 February 2010; published 8 July 2010)

We study continuous-time quantum walks mimicking the quantum search based on Grover's procedure. This allows us to consider structures, that is, databases, with arbitrary topological arrangements of their entries. We show that the topological structure of the database plays a crucial role by analyzing, both analytically and numerically, the transition from the ground to the first excited state of the Hamiltonian associated with different (fractal) structures. Additionally, we use the probability of successfully finding a specific target as another indicator of the importance of the topological structure.

DOI: 10.1103/PhysRevA.82.012305 PACS number(s): 03.67.Lx, 05.60.Gg

I. INTRODUCTION

In the past two decades quantum computation has attracted growing interest, encouraged by the development of tools for the manipulation of single quantum objects, as well as by several remarkable theoretical findings [1]. Different systems have been proposed as candidates for quantum computing; they are based, for instance, on cavity-laser atoms, Bose-Einstein condensates, or NMR techniques (see, e.g., [2–4]). At the same time, a number of quantum algorithms have been designed and some have been shown to be even exponentially faster than their best classical counterparts [5]. In particular, quantum search algorithms, although able to achieve "only" a polynomial speedup, have been proved to be very promising and of widespread use in quantum computation [6,7].

One of the best known quantum search algorithms is attributed to Grover [8]. The algorithm can find a target within an unsorted database made up of N items using $O(\sqrt{N})$ queries. Due to its broad range of applications and its ability to be effectively used as a subroutine [6,9], Grover's algorithm has been thoroughly investigated and a number of different implementations have been proposed (see, e.g., [4,6,10–16]). Recently, implementations based on continuous-time [11,12] as well as on discrete-time quantum walks [14,18,19] have been introduced: Given that the application of random walks in classical algorithms provided significant advantages for approximations and optimization, one is strongly motivated to study quantum walks as algorithmic tools. At the current stage the aim is not only to achieve similar computational improvements, but also to understand the capabilities of quantum computations.

Here we focus on the approach pioneered by Farhi and Gutmann [11] and further developed by Childs and Goldstone [12], based on continuous-time quantum walks (CTQWs). This implementation provides several important advantages: the algorithm does not need auxiliary storage space and it makes it possible to take into account the geometrical arrangement of the database (the latter being either a physical position space or an efficiently encoded Hilbert space [14]). Indeed, while previous studies just considered the cases of the translationally invariant $\mathbb{Z}^d$ (named d-dimensional periodic lattices by Childs and Goldstone [12] and called hypercubic lattices in statistical physics, the term which we adopt here) and of complete graphs [21], here we extend the investigations to the case of generic structures and analyze how geometrical parameters [e.g., (fractal) dimension or (average) coordination number; see later in this article] affect the dynamics of the CTQW. In [12] it was shown that quantum searches based on CTQWs recover the optimal quadratic speedup on complete graphs and on high-dimensional hypercubic lattices (with dimension $d > 4$), while for low-dimensional ($d < 4$) lattices CTQWs cannot outperform their classical counterpart. Hence, it may appear that $d = 4$ works as a "critical dimension", separating highly performing structures from poorly performing ones. We will show, both analytically and numerically, that the dimension of the substrate is not sufficient for getting a sharp transition from the ground to the first excited state; we also take into account the success probability $\pi_{w,s}(t)$, that is, the probability of finding the quantum walker at the target site w at time t, given as initial state the equally weighted superposition s: An efficient quantum walk gives rise to a success probability close to 1 already at very small times t. In particular, we will take into account several kinds of structures: translationally invariant structures, such as d-dimensional hypercubic lattices; complete graphs; fractals with low fractal dimension like dual Sierpinski gaskets and T fractals; hierarchical structures, such as Cayley trees; and structures with (fractal) dimensions larger than four, such as Cartesian products between Euclidean lattices and dual Sierpinski gaskets (for the precise definitions of these structures and of the fractal dimension considered here, see later in this article). In this way we are able to show that for translationally invariant structures with high dimensions, $\pi_{w,s}(t)$ displays sharp peaks, while for fractals or low-dimensional structures the peaks are low and broad so that the quantum walk is not particularly effective in the sense that there exists only a low probability $\pi_{w,s}(t)$ for any t. Moreover, for any structure, we evidence interference phenomena which give rise to a nonmonotonic time dependence of the $\pi_{w,s}(t)$;

*elena.agliari@fis.unipr.it

 ©2010 The American Physical Society

such effects can be significant and must be properly taken into account when considering applications.

Interestingly, the CTQW Hamiltonian used in the quantum search also describes, in solid-state physics, the dynamics of a tight-binding particle in the presence of static, substitutional impurities. In this context our results show that in regular, highly connected geometries (such as the high-dimensional tori) the probability of finding the moving particle at the impurity site is (quasi-) periodic in time and that the localization can be very effective.

Our article is structured as follows. In Sec. II we first review basic principles concerning Grover's search and we explain how it can be implemented by means of CTQWs. In Sec. III we describe the structures used as substrate for the CTQW. Then, in Sec. IV A we present several analytical results, later corroborated and deepened in Sec. IV B, where our numerical results are shown. In Sec. V we focus on the success probability. Finally, Sec. VI contains our conclusions and discussion. In Appendixes A, B, and C we report the details of our analytical calculations.

II. QUANTUM WALKS AND GROVER'S SEARCH

Grover's search algorithm [8] is meant to solve the unsorted search problem under the assumption that there exists a computational oracle working as a black-box function able to decide whether a candidate solution is the true solution. Hence, the oracle knows which is the target among the N entries. The task is to find a target w using the fewest calls to the oracle. While the classical algorithm requires exhaustive searches implying $O(N)$ queries, Grover's algorithm is able to find w using $O(\sqrt{N})$ queries, giving rise to a quadratic speedup [6,20].

A short outline of the idea behind Grover's algorithm in the presence of a single marked target is as follows: First of all, one associates each of the N index integers with a unique orthonormal vector $|x\rangle = |1\rangle, |2\rangle, \ldots, |N\rangle$ in an N-dimensional Hilbert space. Then, one chooses as initial state

$$|s\rangle = \frac{1}{\sqrt{N}} \sum_{x=1}^{N} |x\rangle, \tag{1}$$

which is delocalized over the entire set of states $|x\rangle$ with equal weights at every site x. This is the least biased initialization one can arrange, given the available information (since each of the N nodes is in principle equally likely to be the target index, the initial state is prepared as an equally weighted superposition of all N indices).

Now, to perform the search, one needs to make the state $|s\rangle$ evolve into a state that has almost all the amplitude concentrated in just the $|w\rangle$ component. In such a way a single final measurement will find the system in the state $|w\rangle$, hence revealing the identity of the target index. More precisely, we need an evolution operator whose repeated application makes the amplitude of $|w\rangle$ grow with the number of iterations [6]. This task was originally accomplished within the standard paradigm for quantum computation [8], namely, using a discrete sequence of unitary logic gates, while in the last years several different implementations have been introduced in which the state of the quantum register evolves continuously under the influence of a driving Hamiltonian [13,21,22]. In particular, here we follow the approach developed by Childs and Goldstone [12] which relies on CTQW [11]. As already mentioned, due to their versatility, CTQWs allow to model any discrete database. In fact, a generic discretizable database can be represented by a graph $\mathcal{G} = \{V, E\}$ made up of a set of nodes $V = \{1, 2, \ldots, N\}$, each corresponding to a different item, and of a set of links E joining nodes pairwise in such a way that the topology of the graph mirrors the arrangement of the database. The graph $\mathcal{G}$ can be algebraically described by the adjacency matrix $\mathbf{A}$ whose entry A_{ij} equals one if nodes i and j are connected; otherwise it is zero (also for the diagonal elements). From $\mathbf{A}$ one can directly calculate the degree matrix $\mathbf{Z}$, which is a diagonal matrix with elements $Z_{ij} = z_i \delta_{ij}$, where $z_i = \sum_{j \in N} A_{ij}$ is the coordination number (or degree) of the ith node, that is, the number of its nearest neighbors.

CTQWs on a graph are defined by the Laplacian matrix $\mathbf{L} = \mathbf{Z} - \mathbf{A}$ and obey the following Schrödinger equation for the transition amplitude $\alpha_{k,j}(t)$ from state $|j\rangle$ to state $|k\rangle$ [17]:

$$\frac{d}{dt}\alpha_{k,j}(t) = -i \sum_{l=1}^{N} H_{kl}\alpha_{l,j}(t), \tag{2}$$

where the Hamiltonian is just given by $\mathbf{H} = \mathbf{L}$; therefore, the time is dimensionless and given in units of the coupling elements H_{kl}. The formal solution for $\alpha_{k,j}(t)$ can be written as

$$\alpha_{k,j}(t) = \langle k| \exp(-i\mathbf{H}t)|j\rangle, \tag{3}$$

and its magnitude squared provides the quantum mechanical transition probability $\pi_{k,j}(t) \equiv |\alpha_{k,j}(t)|^2$. Notice that $\mathbf{L}$ is symmetric and non-negative definite; its ground state, corresponding to eigenvalue 0, is given by $|s\rangle$.

Due to the unitary time evolution generated by $\mathbf{H}$, CTQWs are symmetric under time-inversion, which precludes $\pi_{k,j}(t)$ from attaining equipartition at long times. This is different from the behavior of classical continuous-time random walks. Moreover, CTQWs keep memory of the initial conditions, as exemplified by the occurrence of (quasi-) revivals [23,24].

Now, the "oracle Hamiltonian" is given by

$$\mathbf{H}_w = -|w\rangle\langle w|, \tag{4}$$

whose ground state, with energy -1, is just the marked item $|w\rangle$; all other states have energy zero [21]. Then, the Hamiltonian $\mathbf{H}$ governing the time evolution of the quantum walk is

$$\mathbf{H} = \gamma\mathbf{L} + \mathbf{H}_w, \tag{5}$$

where γ is a tunable parameter with units of inverse time, hence dimensionless here.

The *success probability* $\pi^{\gamma}_{w,s}(t)$ is defined as (see also [12])

$$\pi^{\gamma}_{w,s}(t) \equiv |\langle w| \exp(-i\mathbf{H}t)|s\rangle|^2, \tag{6}$$

that is, as the transition probability to be at time t at the target w when starting in the delocalized state $|s\rangle$.

Here we study its dependence on time t and on the parameter γ and we especially aim to evidence the existence of an optimization parameter $\gamma_{\max}$, possibly depending on time, which maximizes $\pi^{\gamma}_{w,s}(t)$. Notice that, having fixed γ, the time t can be measured in terms of the number of queries of the discrete Grover oracle [16].

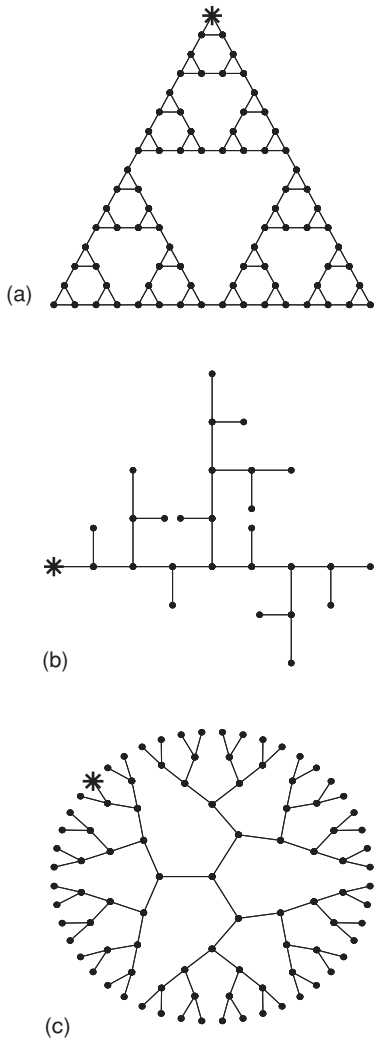

FIG. 1. Examples of fractal structures considered here; in general, the star indicates the position of the trap. (a) Dual Sierpinski gasket of generation 4 and volume $N = 3^g = 81$; due to symmetry, the three corners are equivalent. (b) T fractal of generation 3 and volume $N = 3^g + 1 = 28$; due to the symmetry, all outmost sites (at distance 2^{g-1} from the central node) are equivalent. (c) Cayley tree of generation 5 and volume $N = 3 \times 2^g - 2 = 94$; all of the $N/2 + 1$ outmost sites are equivalent.

III. FRACTAL AND HIERARCHICAL STRUCTURES

Before proceeding, it is worth introducing the geometrical structures on which we are focusing, first the dual Sierpinski gasket (DSG), the T fractal (TF), and the Cayley tree (CT); examples of these structures are shown in Figs. 1(a), 1(b), and 1(c), respectively. Notice that these structures differ significantly from those analyzed previously: While hypercubic lattices with periodic boundary conditions (toroids) are translationally invariant, the aforementioned structures are not.

The DSG, TF, and CT can be built iteratively; at the gth iteration we have the fractal of generation g (see, e.g., [26,29,30]). The DSG and the TF are examples of exactly decimable fractals for which the fractal dimension, d_f, and the spectral dimension, $\tilde{d}$, are exactly known. While the fractal dimension relates the number of nodes inside a sphere to the radius of the sphere [31], the spectral dimension is obtained from the scaling of the eigenmodes of a given structure (phonons for lattices, fractons for fractal substrates) [32], most simply seen in the probability of a random walker to be (still or again) at the original site [33].

Here, we have, namely, $d_f = \ln 3/\ln 2 \approx 1.585$ and $\tilde{d} = 2\ln 3/\ln 5 \approx 1.365$ for the DSG and $d_f = \ln 3/\ln 2$ and $\tilde{d} = 2\ln 3/\ln 6 \approx 1.226$ for the TF. We recall that for the usual, translationally invariant lattices the spectral and fractal dimensions coincide with the Euclidean dimension d, namely, $\tilde{d} = d_f = d = 1$ for the chain, $\tilde{d} = d_f = d = 2$ for the square lattice, and so on. On the other hand, on fractal structures $\tilde{d}$ often replaces d when dealing with dynamical and thermodynamical properties [27]. Also, for fractals $\tilde{d} < d_f$ and d_f is smaller than the Euclidean dimension of the embedding space, that is, 2 for DSG and TF. The CT is no fractal in the classical sense, since its growth with increasing generation is exponential. However, the CT is built in a hierarchical manner, analogous to the TF. We also notice that both the TF and the CT are trees (and are hence devoid of loops) and exhibit a large number $O(N/2)$ of end nodes.

As we will show in the following, CTQW on the DSG, the TF, and the CT can display a low probability $\pi^{\gamma}_{w,s}(t)$ for any t and γ when compared with the case of the translationally invariant lattices, especially when the dimension of the lattice becomes larger than 4. Therefore, one can ask whether the probabilities $\pi^{\gamma}_{w,s}(t)$ can be improved by adopting (fractal or hierarchical) substrates which display a large spectral dimension and a large coordination number.

For instance, we can build up such structures by combining the DSG and Euclidean lattices by means of Cartesian products. In general, the Cartesian product of two graphs $\mathcal{G}_1 = \{V_1, E_1\}$ and $\mathcal{G}_2 = \{V_2, E_2\}$ is a graph $\mathcal{G} = \mathcal{G}_1 \times \mathcal{G}_2$ with the vertex set $V_1 \times V_2$ and such that two nodes (x_1x_2, y_1y_2) are adjacent if $(x_1, y_1) \in E_1$ and $x_2 = y_2$ or $x_1 = y_1$ and $(x_2, y_2) \in E_2$. It has been shown [35] that the spectral dimension $\tilde{d}$ on the product graph $\mathcal{G}$ is then the sum of the corresponding dimensions of the two initial graphs $\tilde{d}_1$ and $\tilde{d}_2$.

We combine in this way the DSG with the chain L_1, with the square lattice L_2, and with the cubic lattice L_3 to obtain more complex structures displaying spectral dimensions approximately equal to 2.365, 3.365, and 4.365, respectively.

Finally, it should be underlined that, dealing with such structures, the location of the target, that is, the node w, also (quantitatively) matters. In the numerical analysis of Sec. IV B, we place the target on a peripheral site, which means, without loss of generality, the apex for the DSG, the leftmost site for the TF, and an outmost site for the CT (see Fig. 1). We expect that a peripheral position for the target site does not correspond to an optimal situation and, since *a priori* the target position is unknown, this choice prevents an overestimation of the probability of finding the target.

IV. OVERLAPS AND TRANSITION

Let us consider the Hamiltonian of Eq. (5) and denote the corresponding set of eigenstates and eigenvalues by $\{|\psi_k\rangle\}$ and $\{E_k\}$, respectively. Now, for large γ the contribution of $\mathbf{H}_w$ to $\mathbf{H}$ is negligible and the ground state $|\psi_0\rangle$ is close to $|s\rangle$. On the other hand, as $\gamma \to 0$ the ground state is close to $|w\rangle$ since the weight of $\mathbf{L}$ is small and, from perturbation theory, we expect

that $|s\rangle$ is close to $|\psi_1\rangle$, that is, to the first excited state of $\mathbf{H}$ [12].

As pointed out by Childs and Goldstone [12], there exists an intermediate range of γ where, for complete graphs and hypercubic lattices with dimension $d > 4$, $|s\rangle$ switches from the ground state $|\psi_0\rangle$ to the first excited state $|\psi_1\rangle$; in the very same region of γ the target state $|w\rangle$ switches from a state with large overlap with $|\psi_1\rangle$ to the ground state $|\psi_0\rangle$. Therefore, by varying γ, we can find a particular value for γ for which the Hamiltonian $\mathbf{H}$ can evolve the state $|s\rangle$ into a state close to the target state $|w\rangle$. The existence and the narrowness of such a range for γ are crucial for a large success probability.

A. Analytical results

As anticipated, the CTQW under study can yield effective results if the Hamiltonian $\mathbf{H}$ is able to rotate the state $|s\rangle$ to a state with a large overlap with $|w\rangle$. For this to occur a first condition which needs to be fulfilled is that there exists an intermediate range of γ over which the state $|s\rangle$ has a substantial overlap with both $|\psi_0\rangle$ and $|\psi_1\rangle$. In this section the occurrence of such a condition is investigated analytically for an arbitrary structure, following arguments similar to those exploited in [12] for d-dimensional hypercubic lattices; the details of the calculations are given in Appendixes A and B while here we just report the main results.

First of all, we define $|\phi_k\rangle$ and $\mathcal{E}(k)$, the kth eigenstate and eigenvalue of the Laplacian $\mathbf{L}$, respectively. In the basis of the eigenstates $|\phi_k\rangle$ the target site $|w\rangle$ can be written as

$$|w\rangle = \sum_{k=0}^{N-1} a_k |\phi_k\rangle, \tag{7}$$

where $a_k \equiv \langle w|\phi_k\rangle$.

As derived in Appendix A, once $\xi_j \equiv \sum_{k\neq 0} |a_k|^2/[\mathcal{E}(k)]^j$ is set, the overlap of $|s\rangle$ with the ground state $|\psi_0\rangle$ or with the first nondegenerate excited state $|\psi_1\rangle$ is (depending on γ) limited from below by the same bound. We find, namely,

$$1 > |\langle s|\psi_0\rangle|^2 > 1 - \frac{\xi_2}{N(\gamma-\xi_1)^2} \tag{8}$$

for $\gamma > \xi_1$ and also

$$1 > |\langle s|\psi_1\rangle|^2 > 1 - \frac{\xi_2}{N(\xi_1-\gamma)^2} \tag{9}$$

for $\gamma < \xi_1$.

Now, we define the (size-dependent) critical value $\tilde{\gamma}$ as that value of γ for which

$$|\langle s|\psi_0\rangle|^2 = |\langle s|\psi_1\rangle|^2 \tag{10}$$

is satisfied; that is, the γ value for which the projection of state s onto the ground and the first excited state has the same magnitude. This is particularly interesting in the limit $N \to \infty$, when a level crossing from state $|\psi_0\rangle$ to state $|\psi_1\rangle$ can occur. In fact, we find that if $\xi_2/[N(\xi_1-\gamma)^2]$ converges (at least in the limit $N \to \infty$) to 0 as γ approaches ξ_1 (from different sides), then $|\langle s|\psi_0\rangle|$ and $|\langle s|\psi_1\rangle|$ both approach 1 [see Eqs. (8) and (9)]; namely; a transition occurs at $\gamma = \xi_1$. Notice, however, that the condition for this to occur is in general nontrivial as ξ_1 and ξ_2 both depend on N. In Appendix A we find a sufficient condition in the Laplacian spectrum and, in particular, in Appendix B we prove that such a condition holds for the DSG for which $\mathcal{E}(k)$ is exactly known [26,28,29]; in this case, we find that

$$\xi_1 \leqslant C N^{\alpha+2/\tilde{d}}, \tag{11}$$

and

$$\xi_2 \leqslant C N^{\alpha+4/\tilde{d}}, \tag{12}$$

where α is a parameter depending on the given network. In general, $-1 \leqslant \alpha < 0$; for hypercubic lattices $\alpha = -1$, regardless of their dimension, while for the DSG we can numerically estimate α as being $\alpha \approx -0.9$ (see Appendix A). Therefore, we expect (for DSG) $\tilde{\gamma}$ to be, approximately,

$$\tilde{\gamma} \approx C N^{\alpha+2/\tilde{d}}. \tag{13}$$

This result is consistent up to logarithmic corrections with the critical points found in [12] for the linear chain and the square lattice, namely, $\tilde{\gamma} \sim N$ and $\tilde{\gamma} \sim \log N$, respectively.

Finally, we point out that the critical parameter $\tilde{\gamma}$ provides interesting information in the context of quantum adiabatic computation [13,34]: $\tilde{\gamma}$ represents a threshold below which we can expect $|w\rangle$ to have a large overlap with the ground state.

B. Numerical results

We now consider the three examples of low-dimensional inhomogeneous structures described previously, for which the overlaps of the initial state $|s\rangle$ and of the target state $|w\rangle$ with $|\psi_1\rangle$ and $|\psi_0\rangle$ are shown in Figs. 2–4 for different generations g, as a function of the parameter γ. These plots evidence that

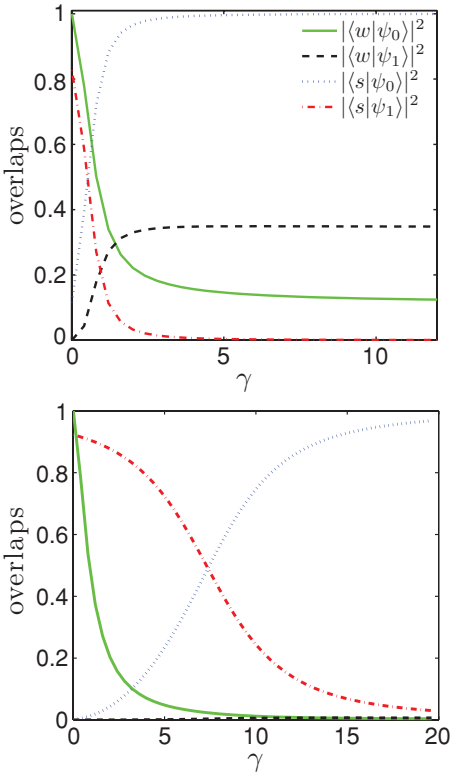

FIG. 2. (Color online) Overlaps for a DSG of generation $g = 3$ (top) and $g = 6$ (bottom) as a function of (the dimensionless) γ. See text for details.

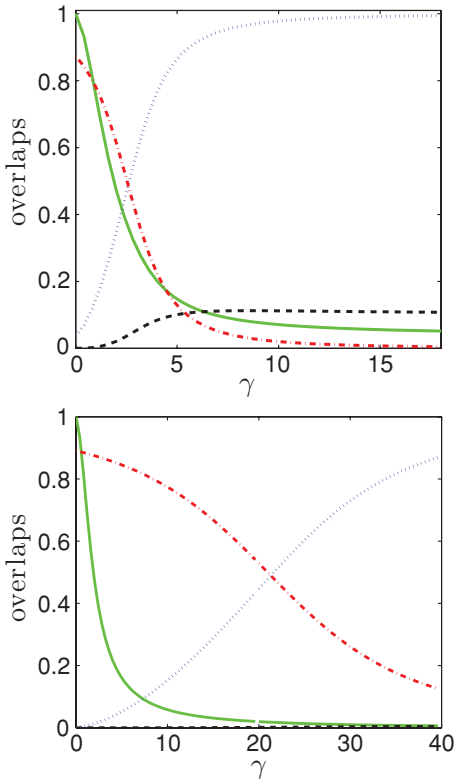

FIG. 3. (Color online) Overlaps for a T fractal of generation $g = 3$ (top) and $g = 6$ (bottom) as a function of γ. The lines are as in Fig. 2.

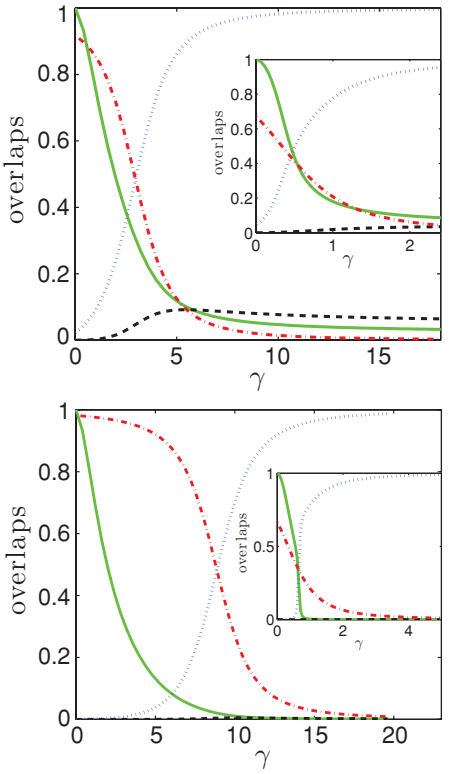

FIG. 4. (Color online) Overlaps for a CT of generation $g = 3$ (top) and $g = 10$ (bottom) as a function of γ. The lines are as in Fig. 2.

there exists an intermediate range of γ where the state $|s\rangle$ changes from having a large overlap with the first excited state to having a large overlap with the ground state. In the same region of γ the overlap $|\langle w|\psi_1\rangle|^2$ is significant for structures of small size (top panels in Figs. 2–4), while it is still very small when the size is large (bottom panels in Figs. 2–4). This is vastly distinct from the situation found for hypercubic lattices [12] where close to $\tilde{\gamma}$ the overlap $|\langle w|\psi_1\rangle|^2$ is significant.

By comparing the plots obtained for the DSG (Fig. 2), the TF (Fig. 3), and the CT (Fig. 4), we notice that $\tilde{\gamma}$ depends sensitively on the underlying topology. In fact, going from DSG to CT and then to TF we notice an amplification of the transition region, which is for TF most spread out, requiring relatively large values of γ in order for $|s\rangle$ to have a large overlap with the ground state. Such effects can be ascribed to the absence of loops and to the existence for TF of a large number of peripheral sites scattered throughout the whole structure which give rise to localization effects [29].

We now calculate $\tilde{\gamma}$ according to Eq. (10) and for several values of g; numerical data and relative best fits are depicted in Fig. 5. For the DSG, numerical points are best fitted by the function $\tilde{\gamma} \approx 3^{0.55g} \approx N^{0.55}$, in very good agreement with the analytical findings. In fact, according to our analytical investigations, $\tilde{\gamma}$ scales with the size of the database like $N^{\alpha+2/\tilde{d}}$ [see Eq. (13)], where, for the DSG, $\alpha + 2/\tilde{d} = \alpha + \log 5/\log 3 \approx 0.57$ (α is taken to equal -0.9). Let us now consider the case of the TF: From numerical data the best fit turns out to be $\tilde{\gamma} \approx 3^{0.70g} \approx N^{0.70}$. Interestingly, this result is still in very good agreement with the analytical approximation of Eq. (13). In fact, for the TF the exponent gets $\alpha + 2/\tilde{d} = \alpha + \log 6/\log 3 \approx 0.73$ (where, again, α is taken to equal -0.9, consistently with the estimates given in Appendix A). Such a consistency might suggest that Eq. (13) is valid not only for the DSG but for any (exactly decimable) fractal with $\tilde{d} < 2$. As for the CT, not being a fractal, Eq. (13) does not hold. Indeed, we find that the value of $\tilde{\gamma}$ corresponding to Eq. (10) grows linearly with the generation of the fractal, namely, logarithmically with N. In Fig. 5 numerical data are fitted by the curve $\tilde{\gamma} = g - 1$ (notice the semilogarithmic plot).

Apart from this, the plots shown in Figs. 2–4 look rather similar. In particular, for networks of large sizes $|\langle w|\psi_0\rangle|^2$ decays with γ more rapidly than $|\langle s|\psi_1\rangle|^2$. Hence, the range of γ over which the transition occurs is wide, analogously to what happens on low-dimensional hypercubic lattices (see [12]). As shown in the next section, this has important effects on the

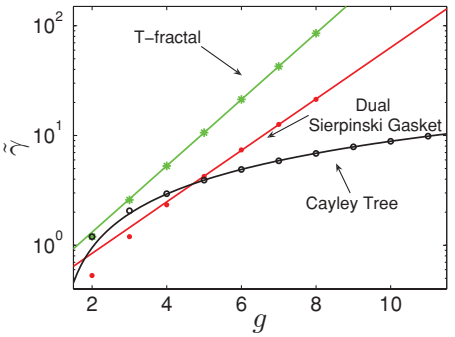

FIG. 5. (Color online) Estimate of $\tilde{\gamma}$ for DSG (red dots), TF (green asterisks), and CT (circles) in a semilogarithmic scale. The continuous lines represent the best fits.

behavior of the success probability and suggests that a sharp transition is associated with an effective search algorithm.

In order to sketch the role of the position of a target we show in the inset of Fig. 4 for the CT of $g = 10$ the case of a target placed on a nearest neighbor of the central node. We see that the transition region is shifted toward lower values of γ. This means that a more central placement of the target is improving the probability for the CTQW to reach the target. Analogous results were also found for DSG and TF. Thus, limiting our focus to peripheral nodes will prevent us from overestimating the success probabilities.

We now consider fractal structures exhibiting large spectral dimension; in particular, we focus on fractals obtained from Cartesian products, such as DSG $\times$ L_1, DSG $\times$ L_2, and DSG $\times$ L_3, as introduced in the previous section. Again, we place the target on a "peripheral site," that is, on a minimally connected site; this displays the coordination numbers 5, 7, and 9, for DSG $\times$ L_1, DSG $\times$ L_2, and DSG $\times$ L_3, respectively. We calculate for these structures the overlaps of the initial state $|s\rangle$ and of the target state $|w\rangle$ with $|\psi_0\rangle$ and $|\psi_1\rangle$; results for DSG $\times$ L_2 ($\tilde{d} = 3.365$) and for DSG $\times$ L_3 ($\tilde{d} = 4.365$) are shown in Fig. 6.

As stressed at the beginning of this section, these plots provide some information about the sharpness of the transition from state $|s\rangle$ to state $|\psi_0\rangle$ and from state $|w\rangle$ to state $|\psi_0\rangle$. However, around $\tilde{\gamma}$ also a significantly large overlap $|\langle w|\psi_1\rangle|^2$ is required.

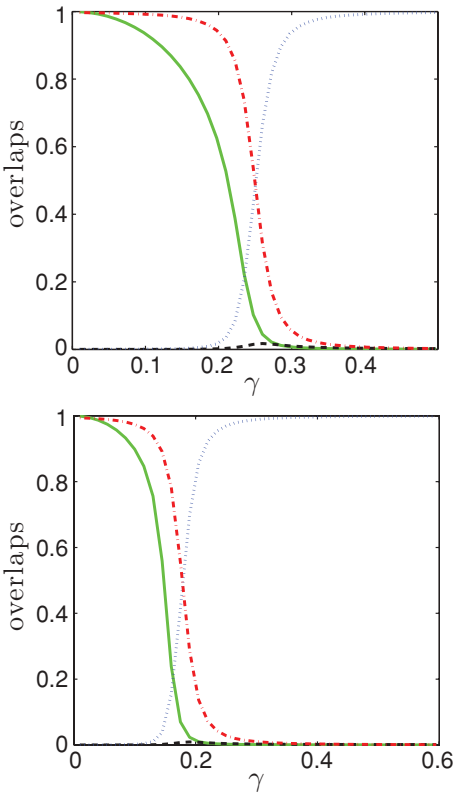

FIG. 6. (Color online) (Top) Overlaps for a DSG $\times$ L_2 structure given by the Cartesian product of a DSG of generation $g = 4$ and a square lattice of size $L = 8$. (Bottom) Overlaps for a DSG $\times$ L_3 obtained from a DSG of generation $g = 4$ and a cubic lattice of size $L = 4$. The lines are as in Fig. 2.

Here the transitions are still rather smooth although, by increasing $\tilde{d}$, the region of γ values, over which the curves representing $|\langle w|\psi_0\rangle|^2$, $|\langle s|\psi_0\rangle|^2$, and $|\langle s|\psi_1\rangle|^2$ intersect, is shrinking. On the other hand, the overlaps between $|w\rangle$ and the first excited state $|\psi_1\rangle$ are negligible for all values of γ.

V. SUCCESS PROBABILITY

We now turn to the success probability $\pi^{\gamma}_{w,s}(t)$ [Eq. (6)] and we investigate numerically its dependence on t and γ. Because of its dependence on time, $\pi^{\gamma}_{w,s}(t)$ carries more information than the previously discussed overlaps.

We first analyze the case of complete graphs and of d-dimensional hypercubic lattices (for which the time dependencies of $\pi^{\gamma}_{w,s}(t)$ have already been determined for special choices of γ in Ref. [12]) before turning to the DSG, the TF, and the CT.

We start our analysis from the complete graph K_N for which, as shown in [12], at $\tilde{\gamma} = 1/N$ the ground state changes sharply from $|s\rangle$ to $|w\rangle$. This transition takes place at $t = \pi\sqrt{N}/2$. Due to the special topology of K_N, we are able to calculate $\pi^{\gamma}_{w,s}(t)$ exactly, obtaining

$$\pi^{\gamma}_{w,s}(t) = \frac{1}{N}\left\{1 + \frac{4(N-1)\sin^2[t\sqrt{4\gamma + (N\gamma - 1)^2}/2]}{4 + \gamma(N - 1/\gamma)^2}\right\}; \tag{14}$$

see Appendix C for details.

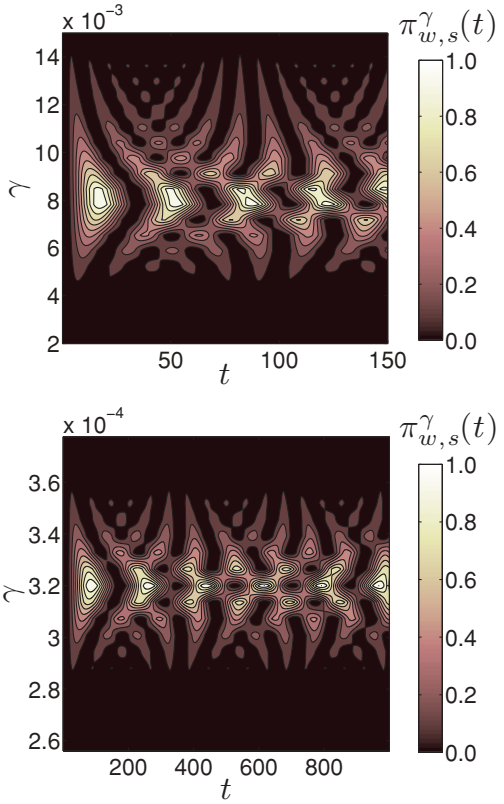

FIG. 7. (Color online) Contour plot of the success probability $\pi_{w,s}(t,\gamma)$ as a function of (the dimensionless) time t and of γ for the complete graph of size $N = 124$ (top) and $N = 3125$ (bottom). One can notice that for $\gamma N = 1$, namely $\gamma = 8.1 \times 10^{-3}$ (top) and $\gamma = 3.2 \times 10^{-4}$ (bottom), $\pi^{\gamma}_{w,s}(t)$ has a period $\tau = \pi\sqrt{124} \approx 35$ and $\tau \approx 176$, respectively.

In Fig. 7 we show $\pi_{w,s}(t,\gamma)$ for the complete graph with $N = 124$ and $N = 3125$. We evaluated the figures both numerically, by first diagonalizing $\mathbf{H}$ in Eq. (6) and projecting on the states $|w\rangle$ and $|s\rangle$, and also by making use of Eq. (14). The results are numerically indistinguishable. From Fig. 7 we see that, around the values $\gamma = 8 \times 10^{-3}$ and $\gamma = 3.2 \times 10^{-4}$ for $N = 124$ and $N = 3125$ respectively, $\pi^{\gamma}_{w,s}(t)$ reaches values very close to 1. In fact, analyzing Eq. (14) (see Appendix C), one finds that $\pi^{\gamma}_{w,s}(t)$ attains its maximal value of 1 for $\gamma N = 1$ and for $t = \pi\sqrt{N}(k + 1/2)$, where $k \in \mathbb{Z}$. Therefore, $\gamma_{\max} = 1/N$. Furthermore, due to the fact that the period between maxima is $T = \pi\sqrt{N}$ for $\gamma_{\max}$, it follows that the CTQW takes $O(\sqrt{N})$ queries to find the target, in agreement with previous results [12,21]. On the other hand, the exact dependence on t and γ also makes it possible to highlight the oscillating behavior of $\pi^{\gamma}_{w,s}(t)$. This means that, although we properly select $\gamma_{\max} = 1/N$, the result for the walk depends sensitively also on t. In particular, for $t = k\pi\sqrt{N}, k \in \mathbb{Z}$, the success probability is minimal and equals $1/N$ (which also corresponds to the absolute minimum).

For the hypercubic lattices the overlaps of the states $|s\rangle$ and $|w\rangle$ with $|\psi_0\rangle$ and $|\psi_1\rangle$ have already been analyzed in [12]; here we display analogous plots (but for larger sizes) in order to compare them with the corresponding success probability $\pi^{\gamma}_{w,s}(t)$. In Fig. 8 we consider the case of a five-dimensional torus (i.e., a five-dimensional cubic lattice with periodic boundary conditions) of linear size $L \equiv N^{1/d} = 5$: The transition at $\tilde{\gamma} \approx 0.12$ is very clear (see the top panel) and

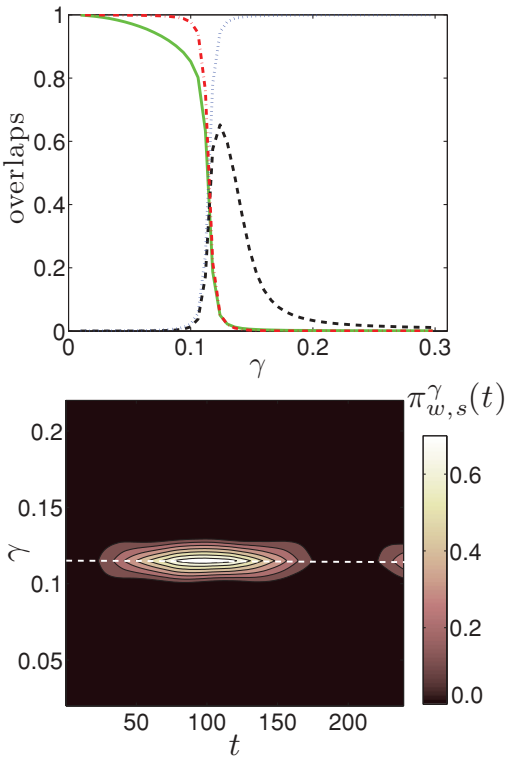

FIG. 8. (Color online) Five-dimensional torus with linear size $L = 5$. (Top) Overlaps (symbols are as in Fig. 2). (Bottom) Contour plot of the success probability $\pi_{w,s}(t,\gamma)$ as a function of t and of γ; the dashed white line represents $\tilde{\gamma} \approx 0.12$.

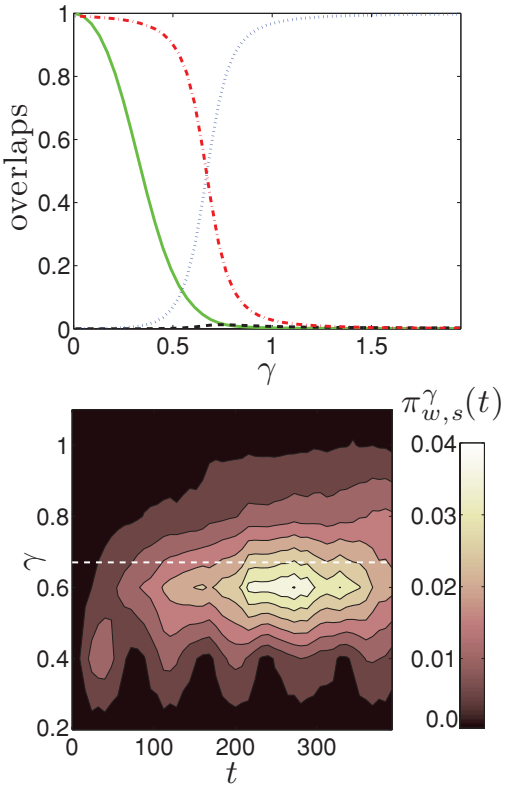

FIG. 9. (Color online) Two-dimensional square torus of linear size $L = 56$. (Top) Overlaps (lines are as in Fig. 2). (Bottom) Success probability as a function of time and γ; the dashed white line represents $\tilde{\gamma} \approx 0.67$.

the success probability is sharply peaked just at $\gamma_{\max} \approx \tilde{\gamma}$ (see the bottom panel).

Away of the critical point $\tilde{\gamma}$ the success probability quickly decays as a function of γ: It is just in the region of largest overlap between the initial state $|s\rangle$ and the target state $|w\rangle$ (namely around $\tilde{\gamma}$) where one expects an optimal success probability.

Again, we notice that $\pi^{\gamma}_{w,s}(t)$ oscillates in time; for $L = 5$ and $\gamma = \gamma_{\max}$ the success probability ranges from about 0 to about 0.8. Moreover, for a given time t, $\pi^{\gamma}_{w,s}(t)$ decays very fast as $|\gamma - \gamma_{\max}|$ increases. For instance, $\pi^{0.9\gamma_{\max}}_{w,s}(70)/\pi^{\gamma_{\max}}_{w,s}(70) \approx 0.05$. As a result, the computational procedure for this structure can be very efficient, provided that the parameter γ can be sensitively controlled.

For hypercubic lattices of dimension $d = 4$, $d = 3$, and $d = 2$ (only the latter case is depicted in Fig. 9), the peaks get more and more broadened and are of smaller magnitude. Notice that the low peaks obtained are in agreement with the analytical results found in [12] which predict for the two-dimensional torus a vanishing success probability for $N \to \infty$.

We now turn to the analysis of the success probability for the DSG, TF, and CT, represented in Figs. 10, 11, and 12, respectively; the top panels display the situation for small networks, the bottom panels for larger networks. First of all, we notice that, as previously found for regular lattices [12], and also for DGS, TF, and CT, $\pi^{\gamma}_{w,s}(t)$ exhibits peaks which are lower and lower as the size N is enlarged. Moreover, for small sizes (top panels) $\gamma_{\max} \approx \tilde{\gamma}$, namely, the maxima

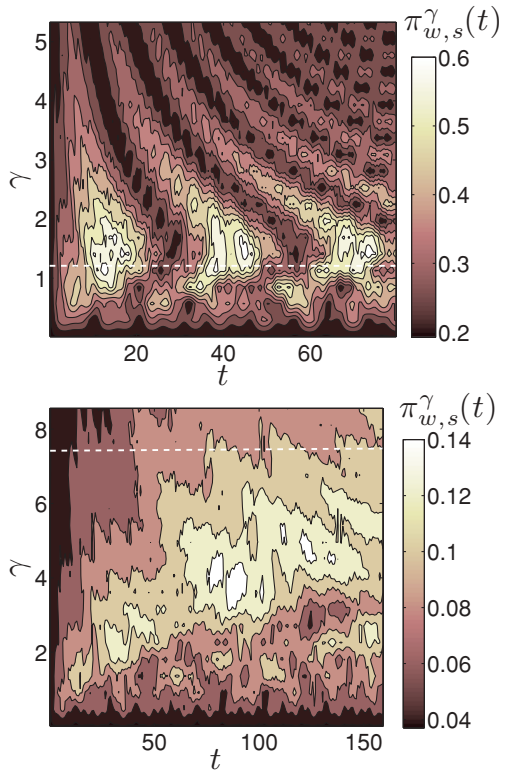

FIG. 10. (Color online) Contour plot of $\pi^{\gamma}_{w,s}(t)$ for the DSG of generation $g = 3$ (top) and $g = 6$ (bottom); the "critical" values $\tilde{\gamma}$ are represented by the dashed line: $\tilde{\gamma}(3) \approx 1.20$ and $\tilde{\gamma}(6) \approx 7.38$ (see Fig. 2).

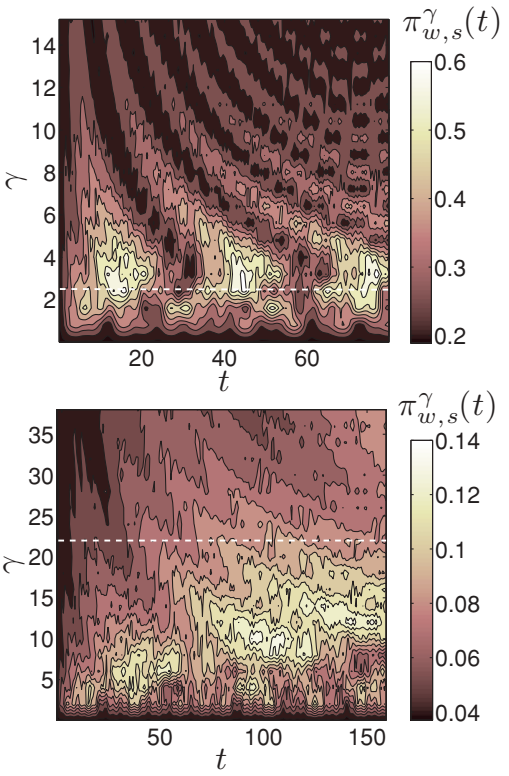

FIG. 11. (Color online) Contour plot of $\pi^{\gamma}_{w,s}(t)$ for the TF of generation $g = 3$ (top) and $g = 6$ (bottom); notice that $\tilde{\gamma}(3) \approx 2.59$ and $\tilde{\gamma}(6) \approx 21.31$ (see Fig. 3).

for the success probability occur for values of γ which are approximately equal to $\tilde{\gamma}$. On the other hand, for large sizes (bottom panels), in the temporal range considered here, $\tilde{\gamma}$ provides an upper bound for $\gamma_{\max}$. However, the most striking feature which emerges from the comparison between the contour plot of the success probability for translationally invariant structures (see Figs. 8 and 9) and for fractal or hierarchical structures (see Figs. 10–12) is that for the latter $\pi_{w,s}(t)$ is much more rough and broadened.

Now it is worth comparing the five-dimensional torus of Fig. 8, the square torus of Fig. 9, and the CT of Fig. 12 since all three are of comparable size N. From the computational point of view, the five-dimensional torus corresponds to the best situation: $\pi^{\gamma}_{w,s}(t)$ is sharp and reaches its maximum value around 0.8 after approximately 100 unit steps; the CT displays a success probability around 0.12 after 150 time steps; the two-dimensional torus corresponds to an ineffective candidate situation: After 300 time steps the peak is still less than 0.1.

In order to compare also to structures with spectral dimensions larger than four, we show in Fig. 13 the success probabilities $\pi^{\gamma}_{w,s}(t)$ for the Cartesian products of a DSG of generation $g = 3$ and a square lattice of size $L = 8$, as well as a cubic lattice of size $L = 8$. Although the maxima of the success probabilities are in both cases larger than the ones for the structures with low dimensions, they show still a fairly irregular pattern. This is in contrast to the highly regular structure of the five-dimensional torus (see Fig. 8).

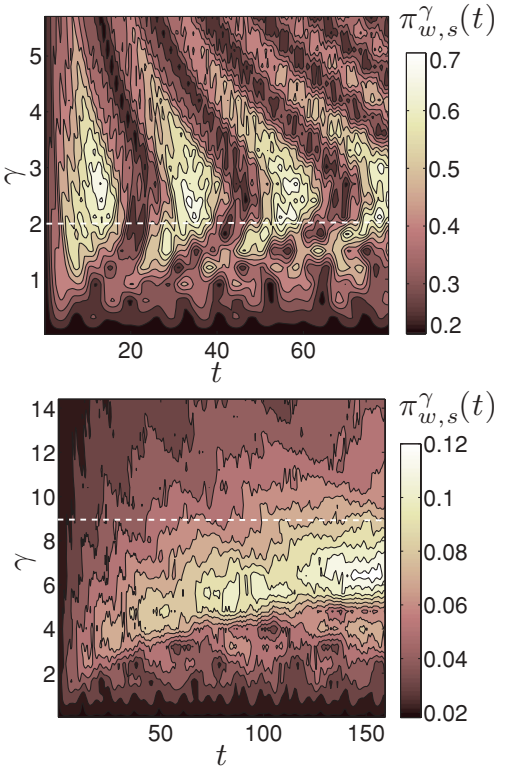

FIG. 12. (Color online) Contour plot of $\pi^{\gamma}_{w,s}(t)$ for the CT of generation $g = 3$ (top) and $g = 10$ (bottom); notice that $\tilde{\gamma}(3) \approx 2.06$ and $\tilde{\gamma}(10) \approx 8.87$ (see Fig. 4).

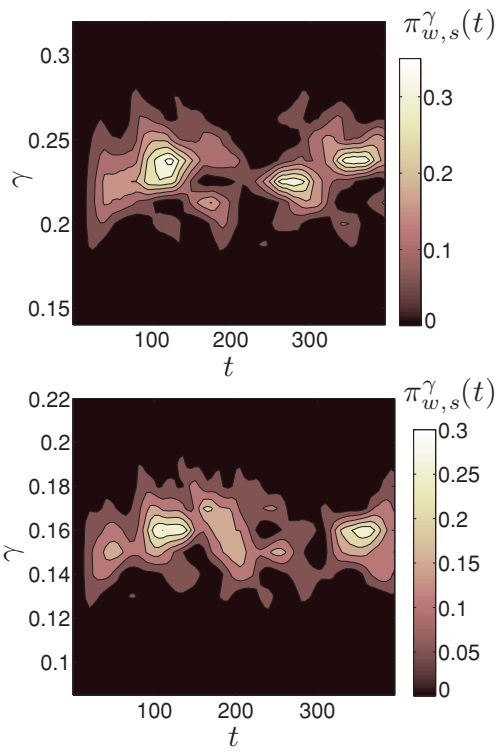

FIG. 13. (Color online) Contour plot of $\pi^{\gamma}_{w,s}(t)$ for the Cartesian product of a DSG of generation $g = 3$ and a square lattice of size $L = 8$ (top) and a cubic lattice of size $L = 8$ (bottom).

Finally, we stress that, as a result of interference phenomena, $\pi^{\gamma}_{w,s}(t)$ oscillates with time. This has some important consequences: Although we can determine and set the optimal $\gamma_{\max}$, the probability of the CTQW reaching the target depends on the instant of time at which it is calculated. In particular, oscillations are "faster" for systems of smaller size; for example for the complete graph we find a period $\tau(\gamma) = 2\pi/\sqrt{(\gamma N - 1)^2 + 4\gamma}$ [see Eq. (14)], namely, $\tau(\gamma_{\max}) = \pi\sqrt{N}$, while for the five-dimensional torus the numerical analysis makes it possible to estimate a period τ which grows exponentially with the lattice size L; for $L = 5$ we get $\tau \approx 200$ (see Fig. 8).

VI. CONCLUSIONS AND PERSPECTIVES

In this work we considered CTQWs mimicking Grover's quantum search problem; we especially focused on how the topology of the space over which the walk takes place affects the position and sharpness of the transition of the ground state. Previous studies [12] highlighted that for translationally invariant structures, such as the hypercubic lattices, the quantum walk can be highly efficient for sufficiently high dimensions, that is $d > 4$. However, here we evidence that on generic graphs the dimension does not represent the key geometric parameter; indeed, both the (average) coordination number and the fact that the structure is translationally invariant or not determine the sharpness of the transition. In fact, on the one hand, a high coordination reduces the distance among nodes and increases the possibility of interference effects, on the other hand, (in the absence of a target) translational invariance prevents the emergence of localization effects [29].

In particular, we considered the success probability $\pi^{\gamma}_{w,s}(t)$ (here $|s\rangle$ and $|w\rangle$ are the initial and the target state, respectively) as a function of the computation time t and of a properly tunable parameter γ entering the Hamiltonian. We showed that for highly dimensional ($d > 4$) translationally invariant structures (five-dimensional torus) there exists a narrow range of γ around a specific value $\tilde{\gamma}$ where the ground state $|\psi_0\rangle$ undergoes a transition from having a large overlap with $|s\rangle$ to a state with a large overlap with $|w\rangle$. This corresponds to a sharply peaked success probability: $\pi^{\gamma}_{w,s}(t)$ displays a set of maxima just at $\tilde{\gamma}$; the first one is reached after $O(\sqrt{N})$ queries. Conversely, for structures with low coordination number and/or fractal or hierarchical topology—such as the cubic (L_3) and square (L_2) tori, the DSG, the TF, the CT, and the Cartesian products DSG $\times$ L_2 and DSG $\times$ L_3—the transition from the initial state to the target state takes place over a wider region of γ around the value $\tilde{\gamma}$. As a consequence of such a spread-out transition, the success probability displays broadened peaks whose locations depend on time. Therefore, for the nontranslationally invariant structures considered here, even with large fractal dimension ($\tilde{d} > 4$), the large success probabilities found for high-dimensional periodic lattices are not recovered. These results, in agreement with previous findings [12], highlight a possible connection between the sharpness of the transition occurring at $\tilde{\gamma}$ and the efficiency of the search algorithm. A mathematical, rigorous proof stating whether a sharp transition is a necessary condition for a good algorithm, which is beyond the aim of this article, could provide a very useful tool for further investigations on quantum search algorithms.

For the DSG we also proved that $\tilde{\gamma}$ scales like $N^{2/\tilde{d}+\alpha}$ ($-1 \leqslant \alpha < 0$); interestingly, our results suggest that such a scaling might be generalized to all (exactly decimable) fractals with spectral dimension $\tilde{d} < 2$.

Apart from the deterministic fractals considered here, it will be extremely interesting to also consider disordered structures such as percolation clusters and random graphs characterized by a degree distribution $P(z)$. These networks display a tunable average degree $\langle z \rangle$, which, in principle, can take values ranging from 0 for totally disconnected networks up to N for completely connected networks. According to the results discussed here, we expect that for a sufficiently large $\langle z \rangle$ and for a sufficiently peaked $P(z)$ the transition from the ground state $|s\rangle$ to a state with significant overlap with $|w\rangle$ occurs sharply and that, consequently, the CTQW speeds up.

ACKNOWLEDGMENTS

Support from the Deutsche Forschungsgemeinschaft and the Fonds der Chemischen Industrie is gratefully acknowledged. E.A. thanks the Italian Foundation "Angelo della Riccia" for financial support.

APPENDIX A: GENERIC STRUCTURES

Let us denote by $\{|\phi_k\rangle\}$ and by $\{\mathcal{E}(k)\}$ the sets of eigenstates and of eigenvalues of the Laplacian $\mathbf{L}$, respectively. On the

basis of the eigenstates the state $|w\rangle$ localized at the target site can be written

$$|w\rangle = \sum_{k=0}^{N} a_k |\phi_k\rangle. \tag{A1}$$

Now, let us consider the complete Hamiltonian $\mathbf{H}$ and the corresponding eigenvalue equation for the state labeled a:

$$\mathbf{H}|\psi_a\rangle = (\gamma \mathbf{L} - |w\rangle\langle w|)|\psi_a\rangle = E_a|\psi_a\rangle. \tag{A2}$$

As shown in [12], when one sets $R_a = |\langle w|\psi_a\rangle|^2$, it is possible to write

$$|\psi_a\rangle = \frac{\sqrt{R_a}}{\gamma \mathbf{L} - E_a}|w\rangle \tag{A3}$$

and

$$F(E_a) \equiv \langle w|\frac{1}{\gamma \mathbf{L} - E_a}|w\rangle = 1. \tag{A4}$$

Here we notice that Eq. (A3), and therefore also Eq. (A4), hold when the eigenvalue E_a is *nondegenerate* (for example, this condition is not fulfilled if we place the trap on the central node of the TF and CT). Equations (A3) and (A4) make it possible then to express the overlap of a given state $|\psi_a\rangle$ (with nondegenerate E_a) with $|s\rangle$ as

$$|\langle s|\psi_a\rangle|^2 = \frac{1}{E_a^2 F'(E_a) N} = \frac{R_a}{N E_a^2}, \tag{A5}$$

where

$$F'(E) \equiv \frac{\partial F(E)}{\partial E} = \langle w|\frac{1}{(\gamma \mathbf{L} - E)^2}|w\rangle, \tag{A6}$$

and, in particular,

$$F'(E_a) = \langle w|\frac{1}{(\gamma \mathbf{L} - E_a)^2}|w\rangle = \frac{1}{R_a}, \tag{A7}$$

(see [12] for more details). It is worth underlining that Eq. (A5) found in [12] for hypercubic lattices actually holds for all structures. The topological details are contained in E_a and $F'(E_a)$.

We now proceed with the calculations without making any assumptions on the topology of the database. First, by using Eq. (7) and $a_k a_k^* = |a_k|^2$, we rewrite $F(E)$ as

$$F(E) = \sum_k \frac{a_k a_k^*}{\gamma \mathcal{E}(k) - E} = \sum_k \frac{|a_k|^2}{\gamma \mathcal{E}(k) - E}, \tag{A8}$$

whose derivative is

$$F'(E) = \sum_{k=1}^{N} \frac{|a_k|^2}{[\gamma \mathcal{E}(k) - E]^2}. \tag{A9}$$

For a generic index k, $0 \leqslant |a_k|^2 < 1$; while the lower bound is clear, the upper bound derives from the fact that the eigenstate $|w\rangle$ cannot correspond to any Laplacian eigenstate. For Euclidean lattices Bloch's theorem makes it possible to write $\langle x|\phi_k\rangle = e^{ikx}/\sqrt{N}$ so that $|a_k|^2 = 1/N$, for any k. On the other hand, for a generic connected structure, *a priori*, one can only write $|a_0|^2 = 1/N$, as a consequence of the fact that the Laplacian eigenstate corresponding to the smallest eigenvalue $\mathcal{E}(0) = 0$ is just $|\phi_0\rangle \equiv |s\rangle$. This suggests a proper restriction of the previous upper bound: $\max_{k\neq 0} |a_k|^2 \leqslant C N^{\alpha}$, with $C > 0$ and $-1 \leqslant \alpha < 0$, both depending on the particular topology chosen. In particular, for Euclidean structures, $C = 1$ and $\alpha = -1$ and one expects that the more inhomogeneous the topology, the larger α. By means of numerical calculations we can estimate α: For not too small DSG and TF we find that $\alpha \approx -0.9$ (see Fig. 14).

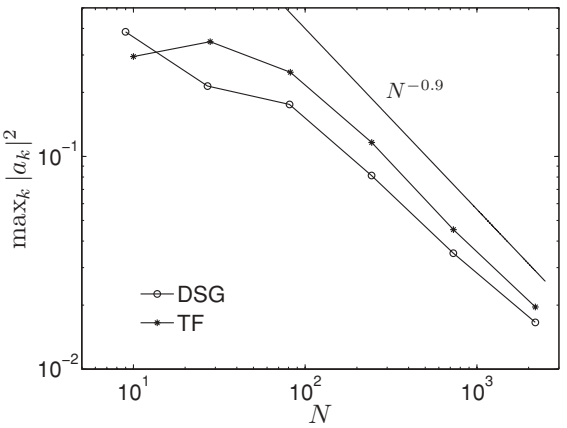

FIG. 14. Numerical estimate of α for the DSG and the TF.

Now, before going on, we define the quantity ξ_j, which will be useful in the following:

$$\xi_j \equiv \sum_{k\neq 0} \frac{|a_k|^2}{[\mathcal{E}(k)]^j} \leqslant C N^{\alpha} \sum_{k\neq 0} \frac{1}{[\mathcal{E}(k)]^j} \equiv C N^{\alpha} \zeta_j, \tag{A10}$$

where we set $\sum_{k\neq 0} 1/[\mathcal{E}(k)]^j \equiv \zeta_j$ and used the upper bound $|a_k|^2 \leqslant C N^{\alpha} < 1$; for hypercubic lattices $\xi_j = \zeta_j/N$, which can be approximated by an integral [12].

Using Eqs. (A5) and (A9) the overlap of $|s\rangle$ with the ground state turns out to be

$$\begin{aligned} |\langle s|\psi_0\rangle|^2 &= \left[1 + N E_0^2 \sum_{k\neq 0} \frac{|a_k|^2}{[\gamma \mathcal{E}(k) + |E_0|]^2}\right]^{-1} \\ &> 1 - N E_0^2 \sum_{k\neq 0} \frac{|a_k|^2}{[\gamma \mathcal{E}(k) + |E_0|]^2} \\ &> 1 - \frac{N E_0^2}{\gamma^2} \sum_{k\neq 0} \frac{|a_k|^2}{[\mathcal{E}(k)]^2}, \end{aligned} \tag{A11}$$

where in the first inequality we used that the sum is positive, while in second inequality we used that both $\mathcal{E}(k)$ and $|E_0|$ are positive. From Eqs. (A11) and (A10), we have

$$|\langle s|\psi_0\rangle|^2 > 1 - \frac{N E_0^2}{\gamma^2} \xi_2. \tag{A12}$$

In general, as γ is varied, E_0 is bounded as $0 \leqslant |E_0| \leqslant 1$ and the bounds can be improved by exploiting the following:

$$\begin{aligned} 1 = F(E_0) &= \frac{|a_0|^2}{|E_0|} + \sum_{k\neq 0} \frac{|a_k|^2}{\gamma \mathcal{E}(k) + |E_0|} \\ &< \frac{1}{N|E_0|} + \sum_{k\neq 0} \frac{|a_k|^2}{\gamma \mathcal{E}(k)} = \frac{1}{N|E_0|} + \frac{\xi_1}{\gamma}. \end{aligned} \tag{A13}$$

In fact, we get

$$\frac{1}{N} < |E_0| < \frac{1}{N}\frac{\gamma}{\gamma-\xi_1}, \tag{A14}$$

where for the lower bound we used that the first sum appearing in Eq. (A13) is positive and that $a_0 = a_0^* = 1/\sqrt{N}$.

Now, from Eqs. (A12) and (A14) it follows straightforwardly that

$$1 - |\langle s|\psi_0\rangle|^2 < \frac{\xi_2}{N(\gamma-\xi_1)^2} \leqslant \frac{CN^{\alpha-1}\zeta_2}{(\gamma - CN^{\alpha}\zeta_1)^2}. \tag{A15}$$

Following analogous arguments we find for the first nondegenerate excited state labeled as 1, being E_1 nondegenerate,

$$|\langle s|\psi_1\rangle|^2 > 1 - NE_1^2 \sum_{k\neq} \frac{|a_k|^2}{[\gamma\mathcal{E}(k) - E_1]^2}, \tag{A16}$$

and

$$E_1 < \frac{1}{N}\frac{\gamma}{(\xi_1-\gamma)}, \tag{A17}$$

from which we get

$$1 - |\langle s|\psi_1\rangle|^2 < \frac{\xi_2}{N(\xi_1-\gamma)^2} \leqslant \frac{CN^{\alpha-1}\zeta_2}{(CN^{\alpha}\zeta_1 - \gamma)^2}. \tag{A18}$$

Notice that in this case $\gamma < \xi_1$ due to the fact that $E_1 > 0$.

Now, by comparing Eqs. (A15) and (A18) we can evidence the existence of a critical value $\tilde{\gamma}$ such that when γ approaches $\tilde{\gamma}$ the ground state switches from $|\psi_0\rangle$ to $|\psi_1\rangle$, at least in the limit $N \to \infty$. In fact, if we take $\tilde{\gamma} = CN^{\alpha}\zeta_1$, then in Eqs. (A15) and (A18) we can set $\gamma = (C+\epsilon)N^{\alpha}\zeta_1$, with $\epsilon > 0$ and $\epsilon < 0$, respectively, obtaining

$$1 - |\langle s|\psi_{0,1}\rangle|^2 < \frac{C}{N^{1+\alpha}\epsilon^2}\frac{\zeta_2}{\zeta_1^2}. \tag{A19}$$

Therefore, recalling that $\alpha - 1$, the condition $\zeta_2 = O(\zeta_1^2)$, as $N \to \infty$ is sufficient for $|\langle s|\psi_{0,1}\rangle|^2 \to 1$. Otherwise stated, as γ approaches $\tilde{\gamma}$ from above ($\epsilon > 0$) or from below ($\epsilon < 0$), the overlap of the ground state with $|\psi_0\rangle$ and with $|\psi_1\rangle$, respectively, is close to 1.

APPENDIX B: THE DUAL SIERPINSKI GASKET

The Laplacian spectrum $\mathcal{E}(k)$ for the DSG is exactly known [26,28,29] and we can therefore calculate exactly the quantities ζ_1 and ζ_2, obtaining estimates for the critical parameter $\tilde{\gamma}$.

At a given generation g, the spectrum includes the eigenvalue 3 with degeneracy $m(3,g) = (3^{g-1}+3)/2$, the eigenvalue 5 with degeneracy $m(5,g) = (3^{g-1}-1)/2$, and the eigenvalues λ^+ and λ^- stemming from the eigenvalue λ, belonging to previous generation and both carrying degeneracy $m(\lambda, g-1)$. For each eigenvalue λ the next-generation eigenvalues $\lambda^{\pm}$ are defined according to

$$\lambda^{\pm} = \frac{5 \pm \sqrt{25-4\lambda}}{2}. \tag{B1}$$

Now it follows directly from Eq. (B1) that any couple $1/\lambda^+$, $1/\lambda^-$ sum up as

$$\frac{1}{\lambda^+} + \frac{1}{\lambda^-} = \frac{5}{\lambda}, \tag{B2}$$

and applying this result iteratively to all the couples making up the spectrum we get

$$\begin{aligned}\zeta_1 &\equiv \sum_{k\neq 0}\frac{1}{\mathcal{E}(k)} \\ &= \sum_{j=0}^{g-1}\frac{5^j}{3}\left(\frac{3^{g-j-1}+3}{2}\right) + \sum_{j=0}^{g-1}\frac{5^j}{5}\left(\frac{3^{g-j-1}-1}{2}\right) \\ &= \frac{1}{30}(-3 - 4\times 3^g + 7\times 5^g).\end{aligned} \tag{B3}$$

As for ζ_2, we can implement a similar iterative procedure by noticing that

$$\frac{1}{(\lambda^+)^2} + \frac{1}{(\lambda^-)^2} = \frac{25-2\lambda}{\lambda^2}. \tag{B4}$$

Therefore, ζ_2 is made up of two terms stemming from the first- and second-order contributions, which are, respectively,

$$\begin{aligned}&\sum_{j=0}^{g-1}\frac{5^{j-1}}{3}\frac{(5^j-1)}{2}\frac{3^{g-j-1}+3}{2} \\ &\quad + \sum_{j=0}^{g-1}\frac{5^{j-1}}{5}\frac{(5^j-1)}{2}\frac{3^{g-j-1}-1}{2} \\ &\quad = \frac{55 + 80\times 3^g - 154\times 5^g + 19\times 5^{2g}}{6600}\end{aligned} \tag{B5}$$

and

$$\begin{aligned}&\sum_{j=0}^{g-1}\frac{25^j}{3^2}\frac{3^{g-j-1}+3}{2} + \sum_{j=0}^{g-1}\frac{25^j}{5^2}\frac{3^{g-j-1}-1}{2} \\ &\quad = \frac{-121 - 68\times 3^g + 189\times 5^{2g}}{19800}.\end{aligned} \tag{B6}$$

Subtracting Eqs. (B6) and (B3) we finally get

$$\begin{aligned}\zeta_2 &\equiv \sum_{k\neq 0}\frac{1}{[\mathcal{E}(k)]^2} \\ &= \frac{1}{900}(-13 - 14\times 3^g + 21\times 5^g + 6\times 25^g).\end{aligned} \tag{B7}$$

Now, recalling that $N = 3^g$ and that the spectral dimension of the DSG is $\tilde{d} = 2\ln 3/\ln 5$, we can write $5^g = N^{2/\tilde{d}}$ and obtain expressions for ζ_1 and ζ_2 as a function of just the volume N and the spectral dimension $\tilde{d}$ of the substrate:

$$\zeta_1 = \frac{1}{30}(-3 - 4N + 7N^{2/\tilde{d}}) \sim \frac{7}{30}N^{2/\tilde{d}}, \tag{B8}$$

$$\zeta_2 = \frac{1}{900}(-13 - 14N + 21N^{2/\tilde{d}} + 6N^{4/\tilde{d}}) \sim \frac{1}{150}N^{4/\tilde{d}}, \tag{B9}$$

where the asymptotic expressions hold for large N.

We notice that as $N \to \infty$, ζ_1 and ζ_2 appearing in Eqs. (B8) and (B9) satisfy the condition $\zeta_2 = O(\zeta_1^2)$ found in Appendix A. More precisely, $\zeta_2 \sim \zeta_1^2$, and this is sufficient for $1 - |\langle s|\psi_0\rangle|^2$ and $1 - |\langle s|\psi_1\rangle|^2$ to converge to zero as $N^{-\alpha}$. In particular, from Eq. (B8) and Eqs. (A15) and (A18), the state

$|s\rangle$ is expected to switch from the ground to the first excited state at

$$\tilde{\gamma} \approx C N^{2/\tilde{d}+\alpha}. \tag{B10}$$

As explained in Sec. IV A, the expressions found here for ζ_1 and ζ_2 are consistent with $\zeta_1 = \sum_k 1/[\mathcal{E}(k)]^j \sim N^{2j/d}$ obtained in [12] for lattices. Therefore, and as suggested by the numerical data discussed in Sec. IV B, it is plausible that Eqs. (B8), (B9), and, above all, the expression for the critical parameter $\tilde{\gamma}$ in Eq. (B10) can be extended to arbitrary structures of spectral dimension $\tilde{d} < 2$.

APPENDIX C: THE COMPLETE GRAPH

Let us start from the definition of success probability given in Eq. (6). Now the propagator $\mathbf{U} \equiv \exp(-i\mathbf{H}t)$ can be calculated as

$$U_{k,j} = \sum_{l=1}^{\infty} \frac{(-it)^l}{l!} (\mathbf{H}^l)_{k,j} \tag{C1}$$

and the success probability can be rewritten as

$$\pi_{w,s}^{\gamma}(t) = \frac{1}{N} \left| \sum_{k=1}^{N} U_{k,w} \right|^2. \tag{C2}$$

Hence, in order to calculate the success probability $\pi_{w,s}^{\gamma}(t)$, we need to find the elements corresponding to the wth column of the lth power of the Hamiltonian. For complete graphs, $\mathbf{H}^l$ displays a high degree of symmetry which allows its exact calculation (see, for example, [21] for a similar calculation where the Hamiltonian is provided by the adjacency matrix). Without loss of generality, we can fix $w = N$ so that the Hamiltonian $\mathbf{H}$ is

$$H = \gamma \begin{pmatrix} N-1 & -1 & -1 & \dots & -1 \\ -1 & N-1 & -1 & \dots & -1 \\ -1 & -1 & N-1 & \dots & -1 \\ \vdots & \ddots & & & \vdots \\ -1 & -1 & -1 & \dots & N-1-1/\gamma \end{pmatrix} \tag{C3}$$

and it is easy to see that, regardless of l, $(\mathbf{H}^l)_{i,N} = (\mathbf{H}^l)_{j,N}$, with $i, j < N$. Therefore, Eq. (C2) can be rewritten as

$$\pi_{w,s}^{\gamma}(t) = \frac{1}{N} |(N-1)U_{1,N} + U_{N,N}|^2. \tag{C4}$$

Now our task is to calculate $U_{1,N}$ and $U_{N,N}$, for which we need the entries $(1,N)$ and (N,N) of the lth power of the Hamiltonian; for better readability, we set $a_{1N}(l) \equiv (\mathbf{H}^l)_{1,N}$ and $a_{NN}(l) \equiv (\mathbf{H}^l)_{N,N}$. Thus, from Eq. (C3) we derive the following recursive relations:

$$a_{1N}(l+1) = a_{1N}(l) - a_{NN}(l) \tag{C5}$$

and

$$a_{NN}(l+1) = -(N-1)a_{1N}(l) + (N-1-\gamma^{-1})a_{NN}(l). \tag{C6}$$

From their combination we get

$$a_{1N}(l+2) = (N-\gamma^{-1})a_{1N}(l+1) + \gamma^{-1}a_{1N}(l), \tag{C7}$$

whose solution is

$$a_{1N}(l) = \frac{\gamma}{2^l}\frac{1}{B}[(A+B)^l - (A-B)^l], \tag{C8}$$

with $A = N\gamma - 1$ and $B = \sqrt{A^2 + 4\gamma}$. From Eqs. (C5) and (C8), $a_{NN}(l)$ is also explicitly defined:

$$a_{NN}(l) = \frac{\gamma}{2^l}\frac{1}{B}[(A+B)^l - (A-B)^l]. \tag{C9}$$

Now, according to Eq. (C2), we can calculate $U_{1,N}$ as

$$\begin{aligned} U_{1,N} &= \sum_{l=0}^{\infty} \frac{(-it\gamma)^l}{l!}\frac{\gamma}{2^l}\frac{1}{B}[(A+B)^l - (A-B)^l] \\ &= \frac{\gamma}{B}\{\exp[-it(A+B)/2] - \exp[-it(A-B)/2]\} \\ &= \frac{\gamma}{B}\exp(-itA/2)\left(-2i\sin\frac{tB}{2}\right). \end{aligned} \tag{C10}$$

Analogous calculations lead to

$$\begin{aligned} U_{N,N} = &\frac{\exp(-it/2A)}{B} \\ &\times \left(-2i\gamma\sin\frac{tB}{2} + iA\sin\frac{tB}{2} - B\cos\frac{tB}{2}\right). \end{aligned} \tag{C11}$$

Hence, by inserting Eqs. (C10) and (C11) into Eq. (C4) and performing the summation,

$$\begin{aligned} \pi_{w,s}^{\gamma}(t) = \frac{1}{N}\Bigg\{1 + &\frac{4\gamma(N-1)}{1+4\gamma-2N\gamma+N^2\gamma^2} \\ &\times \sin^2[t(\sqrt{1+4\gamma-2N\gamma+N^2\gamma^2})/2]\Bigg\}, \end{aligned} \tag{C12}$$

which provides the exact success probability for the complete graph of size N as a function of γ and of t. We can notice that $\pi_{w,s}^{\gamma}(t)$ is strictly larger than zero and that it can be equal to 1 when both $t = \pi(2k+1)/\sqrt{1+4\gamma-2N\gamma+\gamma^2N^2}$, with $k \in \mathbb{Z}$, and $4\gamma/(1+4\gamma-2N\gamma+N^2\gamma^2) = 1$ are satisfied. The latter condition holds for $\gamma N = 1$, just consistent with [12]: There it is found that for $\gamma N = 1$ the walk rotates the state from $|s\rangle$ to $|w\rangle$ and that the gap between the corresponding energies is smallest. For $\gamma N = 1$ the first condition reads $t = \sqrt{N}\pi(k+1/2)$. Hence, for the exact γ and at the right time, the success probability is unitary, but for larger volumes the right times get sparser. We also notice that when N is large and $N\gamma \sim 1$, Eq. (C12) can be simply rewritten as

$$\pi_{w,s}^{\gamma}(\bar{t}) \approx \sin^2(t/\sqrt{N}). \tag{C13}$$

From Eq. (C12) we deduce that for a given time $\bar{t}$, $\pi_{w,s}^{\gamma}(t)$ decreases as $|\gamma N - 1|$ gets larger.

[1] I. L. Chuang and M. A. Nielsen, *Quantum Computation and Quantum Information* (Cambridge University Press, Cambridge, UK, 2000).
[2] L. K. Grover, Phys. Rev. Lett. **79**, 325 (1997).
[3] C. Weiss and M. Holthaus, Europhys. Lett. **59**, 486 (2002).
[4] D. Daems and S. Guérin, Phys. Rev. Lett. **99**, 170503 (2007).
[5] P. W. Shor, *Proceedings of the 35th IEEE Symposium on Foundations of Computer Science* (IEEE, Los Alamos, 1994), p. 124.
[6] A. Ambainis, SIGACT News **35**(2), 22 (2004).
[7] A. M. Childs and J. Goldstone, Phys. Rev. A **70**, 042312 (2004).
[8] L. K. Grover, Phys. Rev. Lett. **79**, 325 (1997).
[9] J. Roland and N. J. Cerf, Phys. Rev. A **68**, 062312 (2003).
[10] S. Aaronson and A. Ambainis, in *Proceedings of the 44th IEEE Symposium on Foundations of Computer Science* (IEEE, Los Alamos, 2003), p. 200.
[11] E. Farhi and S. Gutmann, Phys. Rev. A **58**, 915 (1998).
[12] A. M. Childs and J. Goldstone, Phys. Rev. A **70**, 022314 (2004).
[13] J. Roland and N. J. Cerf, Phys. Rev. A **65**, 042308 (2002).
[14] A. Tulsi, Phys. Rev. A **78**, 012310 (2008).
[15] J. P. Dowling, Nature (London) **439**, 919 (2006).
[16] A. M. Childs, E. Farhi, and S. Gutmann, Quantum Inf. Process. **1**, 35 (2002).
[17] J. Kempe, Contemp. Phys. **44**, 307 (2003).
[18] A. Ambainis, J. Kempe, and A. Rivosh, *SODA '05: Proceeding of the Sixteenth Annual ACM-SIAM Symposium of Discrete Algorithms* (Association for Computing Machinery, New York/Society for Industrial and Applied Mathematics, Philadelphia, 2005), p. 1099.
[19] N. Shenvi, J. Kempe, and K. B. Whaley, Phys. Rev. A **67**, 052307 (2003).
[20] C. H. Bennett, E. Bernstein, G. Brassard, and U. Vazirani, SIAM J. Comput. **26**, 1510 (1997).
[21] E. Farhi and S. Gutmann, Phys. Rev. A **57**, 2403 (1998).
[22] E. Farhi, J. Goldstone, S. Gutmann, and M. Sipser, e-print arXiv:quant-ph/0001106.
[23] I. Sh. Averbukh and N. F. Perelman, Phys. Lett. A **139**, 449 (1989).
[24] O. Mülken and A. Blumen, Phys. Rev. E **71**, 016101 (2005).
[25] D. H. Dunlap and V. M. Kenkre, Phys. Rev. B **34**, 3625 (1986).
[26] M. G. Cosenza and R. Kapral, Phys. Rev. A **46**, 1850 (1992).
[27] K. Hattori, T. Hattori, and H. Watanabe, Prog. Theor. Phys. Suppl. **92**, 108 (1987).
[28] A. Blumen and A. Jurjiu, J. Chem. Phys. **116**, 2636 (2002).
[29] E. Agliari, A. Blumen, and O. Mülken, J. Phys. A **41**, 445301 (2008).
[30] B. Khang and S. Redner, J. Phys. A **22**, 887 (1989).
[31] D. ben-Avraham and S. Havlin, *Diffusion and Reactions in Fractals and Disordered Systems* (Cambridge University Press, Cambridge, UK, 2000); S. Redner, *A Guide to First-Passage Processes* (Cambridge University Press, Cambridge, UK, 2001).
[32] S. Alexander, J. Bernasconi, W. R. Schneider, and R. Orbach, Rev. Mod. Phys. **53**, 175 (1981).
[33] S. Alexander and R. Orbach, J. Phys. Lett. **43**, 625 (1982).
[34] G. E. Santoro and E. Tosatti, J. Phys. A **39**, R393 (2006).
[35] W. Woess, *Random Walks on Infinite Graphs and Groups* (Cambridge University Press, Cambridge, UK, 2000).